AGU100 ADVANCING EARTH AND SPACE SCIENCE

Geophysical Research Letters

RESEARCH LETTER
10.1029/2019GL084700

Key Points:
- Ship fuel sulfate content controls have already had a significant impact on shiptracks
- Almost half of shiptracks may be undetected by current methods
- A potential method for retrieving ship emissions using cloud properties is demonstrated

Supporting Information:
- Supporting Information S1

Correspondence to:
E. Gryspeerdt,
e.gryspeerdt@imperial.ac.uk

Citation:
Gryspeerdt, E., Smith, T. W. P., O'Keeffe, E., Christensen, M. W., & Goldsworth, F. W. (2019). The impact of ship emission controls recorded by cloud properties. *Geophysical Research Letters*, *46*, 12,547–12,555. https://doi.org/10.1029/2019GL084700

Received 24 JUL 2019
Accepted 22 OCT 2019
Accepted article online 7 NOV 2019
Published online 7 NOV 2019

The Impact of Ship Emission Controls Recorded by Cloud Properties

Edward Gryspeerdt[1], Tristan W. P. Smith[2], Eoin O'Keeffe[2,3], Matthew W. Christensen[4], and Fraser W. Goldsworth[1,4]

[1]Space and Atmospheric Physics Group, Imperial College London, London, UK, [2]UCL Energy Institute, University College London, London, UK, [3]University Maritime Advisory Services, London, UK, [4]Department of Physics, University of Oxford, Oxford, UK

Abstract The impact of aerosols on cloud properties is one of the leading uncertainties in the human forcing of the climate. Ships are large, isolated sources of aerosol creating linear cloud formations known as shiptracks. These are an ideal opportunity to identify and measure aerosol-cloud interactions. This work uses over 17,000 shiptracks during the implementation of fuel sulfur content regulations to demonstrate the central role of sulfate aerosol in ship exhaust for modifying clouds. By connecting individual shiptracks to transponder data, it is shown that almost half of shiptracks are likely undetected, masking a significant contribution to the climate impact of shipping. A pathway to retrieving ship sulfate emissions is demonstrated, showing how cloud observations could be used to monitor air pollution.

Plain Language Summary Ships often burn heavy fuel oil, typically creating large amounts of particulate pollution, which is known to modify cloud properties. This creates linear cloud formations, known as shiptracks. In this work, we investigate how the occurrence and properties of shiptracks are related to the particulate emissions from individual ships. We show that the introduction of regulation on ship fuel has already produced a dramatic effect on cloud properties, with shiptracks almost disappearing completely in regions where fuel is regulated. With this new information about the particulates produced by specific ships, we also show that many shiptracks are likely undetected by current identification methods. This study also provides a pathway toward measuring ship emissions using satellite data.

1. Introduction

Almost all cloud droplets form on a particle of atmospheric aerosol, acting as a cloud condensation nucleus (CCN). Ships are significant local sources of aerosol, enhancing the local CCN population (Durkee et al., 2000). Increasing CCN can increase the cloud droplet number concentration (N_d), which can increase the cloud reflectivity (Twomey, 1974). An increase in N_d may further modify clouds and precipitation processes, generating additional changes in the radiative and microphysical properties of the cloud field (Albrecht, 1989).

The modification of cloud properties by anthropogenic aerosol has a significant cooling effect on the climate (Boucher et al., 2013), but the magnitude of this effect is uncertain due to the difficulty in isolating the aerosol impact on a cloud from that of the local meteorology (Grandey et al., 2013; Quaas et al., 2010). As point sources of aerosol, ships create linear perturbations in cloud properties, features known as shiptracks (Conover, 1966). As ships are assumed to emit aerosol independently of the large-scale atmospheric conditions, shiptracks are used as "experiments of opportunity," isolating the impact of aerosol on cloud properties (Segrin et al., 2007; Christensen & Stephens, 2011; Christensen et al., 2014; Toll et al., 2017; Gryspeerdt et al., 2019).

Shiptracks are usually found in regions with large amounts of low cloud, such as the western coasts of continents (Schreier et al., 2007). Tracks identified using satellite data typically have lengths of over 100 km (Schreier et al., 2010) and can persist for a number of days and influence much larger areas (Goren & Rosenfeld, 2012) but are not always clearly visible (Possner et al., 2018). Although ships can provide local heat fluxes of up to 30 MW and moisture fluxes of 2 kg/s (Hobbs et al., 2000), a comparison of different ship types during the Monterey Area Shiptrack campaign (Durkee et al., 2000) demonstrated that the aerosol

emissions of the ship were the primary control on the formation of shiptracks (Durkee et al., 2000), with heavy fuel oil (HFO)-powered ships producing stronger cloud perturbations than liquified petroleum gas- or nuclear-powered vessels (Hobbs et al., 2000). However, the aerosol components responsible for shiptracks are unclear, with both Monterey Area Shiptrack campaign and the later E-PEACE (Russell et al., 2013) campaign finding ship effluent dominated by organics.

The implementation of ship fuel sulfur content (FSC) controls provides a way to investigate the role of ship-emitted sulfate aerosol as CCN. FSC is regulated according to standards set by the International Maritime Organization (IMO), with a global limit of 3.5% S (by mass). Two emission control areas (ECAs) are defined, one around the coast of North America and a second covering the North Sea, Baltic Sea, and English Channel (IMO, 2008). In these regions, FSC was unrestricted before 2005 and limited to 1% in 2010 and 0.1% in 2015 (IMO, 2008). In 2020, worldwide restrictions will be introduced, limiting FSC to 0.5% outside the ECAs. Recent advances in ship monitoring using satellites allows the position and speed of ships to be monitored globally (Eriksen et al., 2006), which can be combined with the physical properties of the ship and the FSC to estimate sulfur emissions (Smith et al., 2015).

We use this new satellite data set to connect ship sulfate emissions to shiptrack properties across the ECA regions. Previous studies have been limited to around 1,500 shiptracks globally (Campmany et al., 2009; Toll et al., 2017) and 200 colocations between ships and the associated shiptrack (Durkee et al., 2000). They have often been restricted to a specific season (Coakley et al., 2000; Segrin et al., 2007) or used a small field-of-view instrument (Christensen & Stephens, 2011), and as a result the frequency of their occurrence could not be calculated. In this work, we use multiple years of satellite and reanalysis data to develop a high-density data set of over 17,000 tracks located around ECAs, including almost 1,300 colocations between ships and shiptracks, key for computing how the occurrence frequency of shiptracks relates to meteorological conditions and ship emissions.

2. Methods

2.1. Shiptrack Identification

All the shiptracks in this study are identified manually to limit false detections, using data from the Moderate Resolution Imaging Spectroradiometer (MODIS) Aqua MYD021KM calibrated radiances product and the MYD06_L2 cloud product (Platnick et al., 2017). Shiptracks are initially located using the day microphysics image (Rosenfeld et al., 2014), a composite of visible, near, and thermal infrared channels. This allows shiptracks to be distinguished from other linear features such as contrails. A visible RGB image and the retrieved cloud droplet number concentration (N_d) (Grosvenor et al., 2018; Quaas et al., 2006) is used for further information in uncertain cases. Two regions are investigated, a region covering the ECA region off the coast of California (30–45°N, 115–130°W) and one surrounding the European ECA (42–64°N, 12°W to 8°E). All the daytime MODIS Aqua images intersecting these regions for the years of 2003 and 2015 are examined, along with 2014 and 2016 for the Californian region. Many images only partially intersect this region; shiptracks that occur outside the study region are recorded as long as they are in one of these images.

In total, 11,553 MODIS images are examined and 17,325 tracks are identified; 12,787 of these are in the Californian region and 4,538 in the European region. In the Californian region during 2015, ship positions are determined using the Automated Identification System (AIS), a maritime collision avoidance system. AIS transponders are installed on all ships larger than 300 gross tons, broadcasting identity, position, speed, and other safety information (IMO, 2002). These ship positions are used together with European Centre for Medium-Range Weather Forecasts Reanalysis ERA5 winds to derive 2-D Lagrangian trajectories as estimates of the shiptrack locations, with a 30-min advection time step for 10 hr previous to the satellite overpass. This allows the identification of the generating ship even in cases where there is no clear shiptrack head and there is a significant distance separation between the ship and the shiptrack (the 90th percentile distance is around 100 km). These estimated locations are only used to assist in the manual identification of shiptracks rather than as the sole method of identification. This avoids biases in the driving reanalysis data affecting shiptrack statistics; 1,299 shiptracks are matched to AIS tracks for the year 2015.

The meteorological properties for the shiptrack are characterized at the first location where the shiptrack becomes visible, as this is more representative of the conditions for shiptrack formation than those at the ship, especially if the shiptrack and ship are separated by a significant distance. The properties are from the European Centre for Medium-Range Weather Forecasts Reanalysis-Interim reanalysis, regridded to a 1° by

1° resolution. The MODIS properties used to characterize shiptrack formation are from the MYD06_L2 1 km cloud product, averaged for regions within 30 km of the ship. N_d is calculated using the adiabatic assumption(Quaas et al., 2006) and a temperature correction(Gryspeerdt et al., 2016). The reanalysis background SO_4 is from the Modern Era Retrospective-Analysis for Research and Applications-2 (MERRA2) reanalysis (Randles et al., 2017) at 900 hPa (following McCoy et al., 2017), with the nearest neighbor value from the native resolution product (approximately 0.5° by 0.5°) considered characteristic of the shiptrack.

2.2. Ship Emissions Parametrization

Ship emissions are estimated at the level of individual ships following the bottom-up methodology outlined in the Third IMO Greenhouse Gas Study (Smith et al., 2015). A brief description is given here with further details and validation available in the report. This method combines the ship activity data from AIS with technical data about the ship type, propulsion, and auxiliary power requirements based on the IHS Fairplay database. The resistance to ship motion is assumed to be primarily hydrodynamic, such that it is primarily a function of ship speed and draught. The power requirement is modified by constant factors to account for hull fouling and weather. The SO_x emissions are then estimated by combining the power requirement with a fuel consumption based on engine type and load and FSC (0.1% inside the ECA, 2.5% outside).

The quantified emission uncertainty for the dominant ship types in this study (container and bulk carriers) is approximately 14%. This uncertainty comes primarily from uncertainties in the ship speed and draught, such that it reduces for ships with more regular and complete AIS reports. Additional uncertainty comes from the FSC which is assumed as the global fleet HFO average (≈2.5%). More complete data in the future would be expected to provide a more accurate picture of individual ship SO_x emissions.

Around 11% of identified tracks in the Californian region cannot be clearly linked to an individual ship using the AIS records. This does not mean that 11% of ships are missing from the database, only that they cannot be accurately located in the satellite overpass window.

2.3. Shiptrack Properties

The pixels defining the shiptrack are identified using a modified version of the method in Segrin et al. (2007) and Christensen and Stephens (2011). Each track is split into 20-km segments. For each segment, a linear regression of N_d with cross-track distance (perpendicular to the track direction) is used to identify the background variation of N_d. Points more than 1.67 standard deviations above this background are considered polluted. A new background is calculated without these polluted pixels, and a new set of polluted pixels is identified. This process repeats until the polluted pixels are unchanged between iterations. Regions of polluted pixels intersecting the identified track are considered part of the track; other polluted pixels are removed from the analysis. A background N_d is then calculated from pixels between 4 and 14 km from the edge of the polluted region, excluding any previously identified polluted pixels. Pixels with a solar zenith angle greater than 65° , a 5-km cloud fraction less than 90%, and a subpixel reflectance variability (Cloud_Mask_SPI) greater than 30 are also removed due to the increased retrieval uncertainty in these situations (Grosvenor et al., 2018).

For comparison with the ship emissions estimates, shiptrack properties are restricted to the region within 4 hr of emission (as calculated using the Lagrangian trajectory model). Tracks used for Figure 3 must also contain more than 75 polluted pixels and have a length-normalized Fréchet distance between the observed and estimated track locations of less than 0.75, ensuring the identification of the correct ship for each shiptrack.

3. Results

3.1. Shiptrack Occurrence

The occurrence of shiptracks is controlled by two main factors: the occurrence of suitable low cloud and the presence of a ship emitting aerosol. Figure 1 highlights the impact of both of these factors. In 2003, 2,875 tracks are identified in the northwest Pacific region. These are concentrated close to the coast, particularly in the region between the ports of San Francisco/Oakland (SF) and Los Angeles/Long Beach (LA). Increased concentrations of shiptracks are visible in major shipping lanes leaving Vancouver/Seattle-Tacoma (VST), San Francisco, and Los Angeles. The occurrence of shiptracks is correlated to the liquid cloud fraction, with higher shiptrack occurrence found in regions with a large amount of liquid cloud.

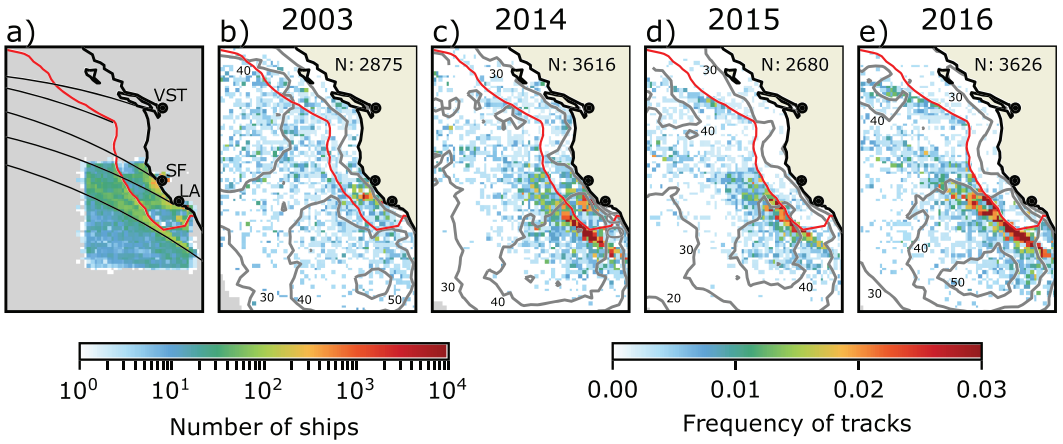

Figure 1. Interannual variation in shiptrack locations. (a) Locations of ships determined using AIS data at the satellite overpass time in 2015. Thin black lines show major shipping routes, and the orange dots the locations of the ports of Vancouver/Seattle, San Francisco/Oakland, and Los Angeles/Long Beach. (b–e) Frequency of occurrence of identified shiptracks for the years 2003, 2014, 2015, and 2016. The red line is the U.S. Pacific ECA. Thin gray lines show the percentage annual average liquid cloud fraction from MODIS. The number of identified tracks each year is in the upper right of each subplot. Land and locations viewed by fewer than 100 granules are masked.

Between 2010 and 2015 (Figure 1c), FSC inside the ECA was limited to 1.0%. This does not produce an obvious change in the occurrence of shiptracks, with no clear change being observed across the boundary of the ECA. A large concentration of tracks is observed along the southwestern corner of the ECA. This may indicate ships avoiding the ECA but it is approximately aligned with the great-circle route between Panama (via False Cape) and Tokyo and so may indicate an increase in activity along a preexisting route. Part of the increase in shiptrack number in this region is due to the anomalously high low cloud coverage close to the coast in 2014 producing conditions more conducive to shiptrack formation (Figure 2a and supporting information Figure S3).

The introduction of the 0.1% FSC limit in the ECA produces a dramatic change between 2014 and 2015, with the almost complete absence of shiptracks in the ECA region, continuing in 2016 (Figures 1d and 1e). The scale of the change is such that it is visible in individual satellite images in 2015 (Figure S1). Although there is a corresponding decrease in the liquid cloud fraction in 2015 (Figures 2a and S3), the similarity of the change inside and outside the ECA means that it cannot explain the relative change in shiptrack frequency. Similarly, there is a change in shipping patterns, with an increase in shiptracks along the edge of the Canadian sector of the ECA being evidence of ships taking a longer route from Vancouver to the Fox Island passes to minimize time spent in the ECA. However, as ship traffic at the main three port locations increased in 2015 (AAPA, 2015), this change in shipping patterns does not explain the reduction in shiptracks, particularly near the ports. A similar reduction in shiptracks is observed in the North Sea/English Channel ECA (Figure S2), but as the frequency of shiptracks in this region is lower due to the higher background pollution, the rest of this work focuses on the Californian ECA. The reduction in shiptracks following the implementation of FSC regulation in the ECA demonstrates the central role of sulfur compounds in generating CCN in shiptracks, despite the large fraction of organics in ship effluent (Hobbs et al., 2000; Russell et al., 2013).

3.2. Meteorological Controls

The dominant control on shiptrack formation is the occurrence of liquid cloud (Figure 2), with 67% of ships forming tracks having a liquid cloud fraction of over 80% (within 30 km of the ship), compared to just 27% of the ships not forming tracks. Once the requirement for liquid clouds is accounted for, there is very little relationship between track occurrence and boundary layer height, low troposphere stability (LTS) (Klein & Hartmann, 1993), or 10-m wind speed, factors previously suggested to be important controls on shiptrack formation (Durkee et al., 2000). Relative humidity (RH) at 850 hPa (close to the cloud top) is strongly correlated with track occurrence, with only 8.5% of tracks forming with an RH greater than 50%. The prevalence of shiptracks in drier conditions may be related to the stronger cloud top radiative cooling in drier conditions promoting stronger in-cloud updraughts (Zheng et al., 2016), increasing cloud sensitivity to aerosol perturbations (Twomey, 1959).

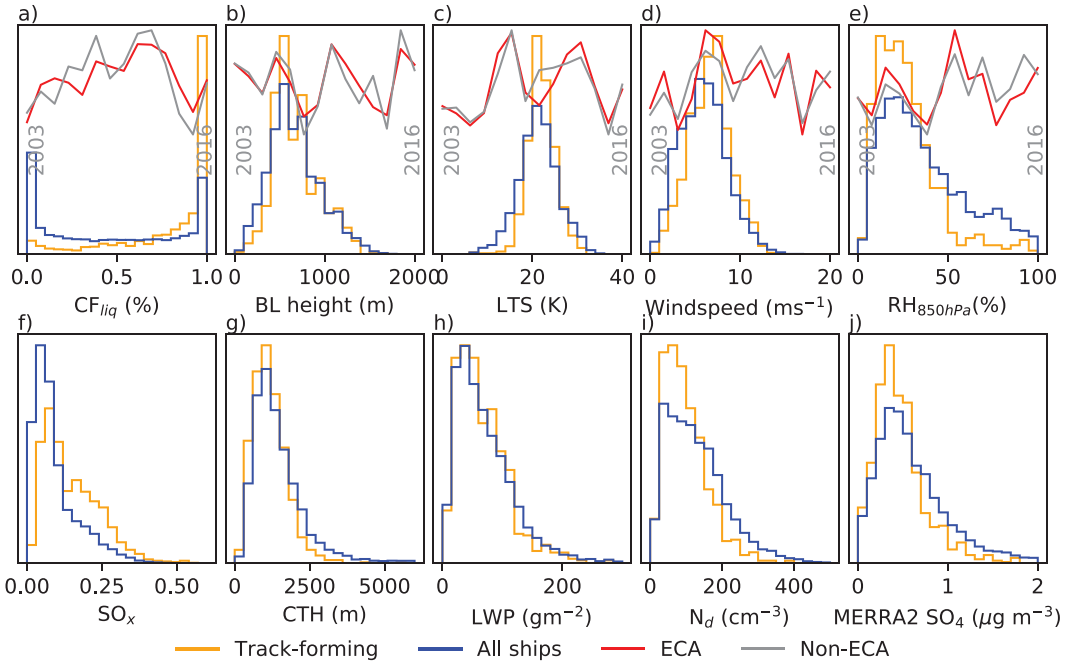

Figure 2. The relationship between meteorology and track formation probability. Histograms of meteorological properties for all ships (blue) and ships forming shiptracks (orange) within the Californian study region during 2015. (a) The liquid cloud fraction within 30 km of the ship, (b) boundary layer height, (c) low troposphere stability, (d) 10-m wind speed, and (e) relative humidity at 850 hPa, determined using ERA-Interim, with a linear interpolation between the nearest 6-hr analysis time steps. (f) The parametrized ship SO_x emissions. The (g) cloud top height, (h) liquid water path, and (i) adiabatic droplet number concentration (averages within 30 km of the ship). (j) Background SO_4 concentration from the MERRA2 reanalysis. For all subplots apart from (a), only cases with greater than 90% liquid cloud fraction are included. The red and gray lines indicate the annual anomaly with respect to the mean of each parameter from 2003 to 2016 within and outside the ECA region, respectively.

Although there is significant interannual variation in the large-scale meteorological properties in the region, there is not a trend in the properties that could explain the reduction of shiptracks in the ECA (Figure 2, gray and red lines). The reduction in liquid CF in 2015 is similar both inside and outside the ECA (Figure 2a). The only variable that shows a significant difference in the anomaly inside compared to outside the ECA is RH_{850hPa}, where a relative decrease within the ECA during 2015 compared to outside would lead to an increase in the fraction of tracks inside the ECA, rather than the observed decrease (Figure 2d).

As with previous studies (Coakley et al., 2000), cloud top height is found to be correlated to shiptrack occurrence, but the relationship weakens once the requirement for a high low-cloud fraction is accounted for (Figure 2g). Similarly, liquid water path, an indication of cloud geometrical thickness, is not strongly correlated with track occurrence (Figure 2i). However, there is a clear impact of the aerosol environment. Using MERRA SO_4 as a measure of the background aerosol (Figure 2j), track formation becomes more common in clean environments (Noone et al., 2000). This is further supported by the strong increase in track formation at low N_d (Figure 2h). Using parametrized ship emissions calculated following the IMO Third GHG Study (Smith et al., 2015) (further details in section 2), it is clear that shiptracks become more common as ship emissions increase (Figure 2f). However, meteorological and background aerosol properties play a central role in controlling shiptrack occurrence.

3.3. Estimating Shiptrack Strength

As a binary criterion, shiptrack occurrence is an imprecise measure of the impact of ship aerosol emissions on cloud properties, with weak tracks being given the same weight as tracks producing a large change in cloud properties. To avoid this issue, the strength of observed shiptracks is characterized using the enhancement factor ($\epsilon_N = N_{pol}/N_{cln}$, equation (1)), where N_{pol} is the N_d inside the shiptrack and N_{cln} the background N_d.

$$\epsilon_N = \frac{N_{pol}}{N_{cln}} = \frac{A_E^{\gamma}}{\alpha + \beta N_{cln}} + 1 \tag{1}$$

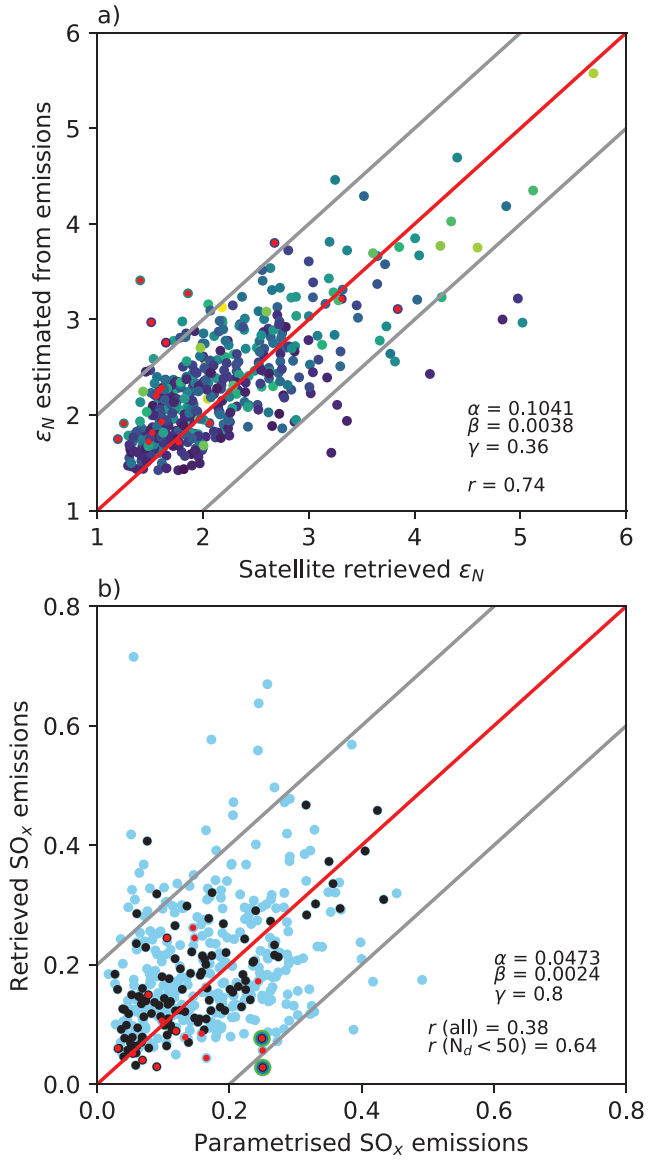

Figure 3. Using ship emissions to estimate shiptrack properties. (a) The measured N_d enhancement (ϵ_N) as a function of the ϵ_N estimated given N_{cln} and the parametrized ship emissions. Colors are the parametrized ship emissions (yellow and blue are high and low SO_x emissions respectively). (b) SO_x emissions retrieved using the shiptrack properties as a function of the parametrized SO_x emissions (section 2.2). Black points have $N_{cln} < 50$ cm^{-3}. Red points in both plots are located in the ECA region. Green circled points are identified biases in the emissions parametrization (section 3.5). α, β, and γ are parameters in equation (1). Note the different fit parameters in (b) due to the nonlinearity of equation (1).

Equation (1) (see supporting information for derivation) is used to fit ϵ_N, where A_E is the parametrized ship SO_x emissions (section 2.2) and α, β, and γ are constants of the fit. Shiptracks are selected from the Californian region in 2015 (as described in section 2.3), reducing the sample size to 420. The ship SO_x emissions alone have only a weak correlation ($r = 0.20$) to ϵ_N, as ϵ_N is strongly controlled by N_{cln}. When ignoring ship SO_x emissions, ϵ_N can be fit with a correlation of 0.63, rising to 0.75 when the ship SO_x emissions are included. This shows the important role of ship emissions in controlling the properties of shiptracks, driving the changes observed in Figure 1.

3.4. The Impact of Undetected Shiptracks

Higher ϵ_N tracks are more easily distinguished from the background, although weaker shiptracks may still exert a significant impact on the climate (Possner et al., 2018). Their ease of identification biases the ϵ_N

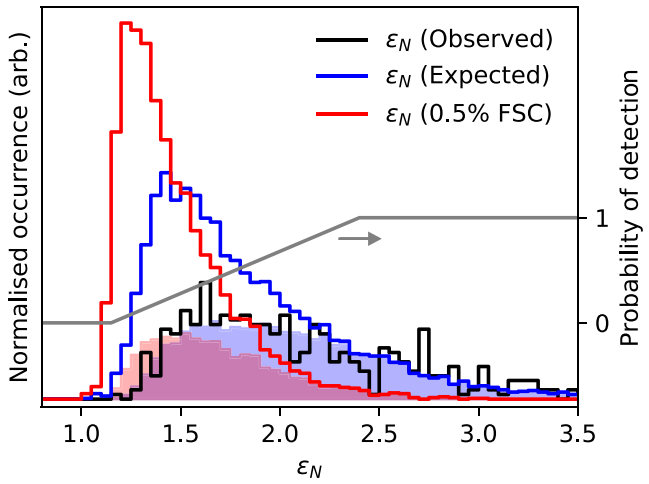

Figure 4. Fraction of visible tracks. The black line is the normalized distribution of ϵ_N (N_{pol}/N_{cln}) from the observed shiptracks included in Figure 3. The blue line is the estimated distribution of ϵ_N using equation (1) for every ship in the Californian region. The red line is the estimated ϵ_N distribution after a reduction to 0.5% FSC (expected in 2020). The filled areas are the ϵ_N distributions of the detected tracks, given the probability of detection (gray line).

in the observed tracks toward larger values, with the 10th percentile at 1.39 (Figure 4). Estimating ϵ_N for each ship in the Californian region using equation (1) and the fit parameters in Figure 3a, it is clear that a larger number of low ϵ_N shiptracks are expected (Figure 4, blue line) than are observed (Figure 4, black line). Normalizing the estimated ϵ_N distribution to the observed distribution to minimize the relative mean squared error yields a probability of detection as a function of ϵ_N (Figure 4, gray line). This assumes that the strongest tracks are always detected. However, as every image in 2015 has been inspected at least twice, the probability of the strongest tracks being missed is likely small. This suggests that almost half (43%) of tracks are undetected in this study (Figure 4, the fraction of the area under the blue line not covered by the blue filled area). With a radiative forcing proportional to the logarithm of ϵ_N (Twomey, 1974), these undetected shiptracks contribute 37% of the total forcing from shiptracks.

The emissions parametrization assumes a FSC of 2.5% outside the ECA (section 2.2). Following equation (1), the implementation of a global 0.5% FSC limit in 2020 is expected to lead to a lower average ϵ_N (Figure 4, red line) and a 51% reduction in the number of detected shiptracks (Figure 4, red area), assuming full compliance with FSC regulations and that other factors such as the cloud fraction and detection probability remain unchanged. Including the estimated contribution from undetected tracks, this implies a 31% reduction in the forcing.

This method suggests that the introduction of the ECA in 2015 would have produced a 73% reduction in the number of shiptracks. Although smaller than the observed 86% decrease (Figure 1), the 10% decrease in liquid cloud fraction from 2014 to 2015 (Figure 2) would explain much of the remaining decrease, building further confidence in this method for estimating the number of detected shiptracks.

There remains significant uncertainty in these estimates, due to the fitting of the estimated ϵ_N distribution to the observed ϵ_N distribution and the poorly constrained radiative properties and spatial extent of these undetected shiptracks. An increase in cloud fraction at high N_{cln} (Gryspeerdt et al., 2016) could lead to shiptracks with a higher N_{cln} (and so lower ϵ_N) having a larger spatial coverage, resulting in a larger contribution from undetected tracks to the overall radiative forcing. Studies into the properties and factors controlling these weaker shiptracks are necessary to improve estimates of their climate impact.

3.5. Retrieving Ship SO_x Emissions

Following equation (1), the ship emissions can potentially be retrieved if ϵ_N is known (Figure 3b). Due to the strong impact of the background state/N_{cln} on ϵ_N, the correlation between the parametrized (section 2.2) and retrieved SO_x emissions is only 0.38. However, if the retrieval is restricted to only cases where N_{cln} <50 cm^{-3}, the correlation rises to 0.64 (Figure 3b, black points), due to the larger ϵ_N and hence greater signal-to-noise ratio at lower values of N_{cln}.

Some of the remaining uncertainty in the retrieval is due to the constant FSC assumed in the emissions parametrization (section 2.2), despite significant global FSC variations in HFO. The retrieval identified two cases where the emissions parametrization considered ships as outside the ECA, when they were actually inside (Figure 3b, points circled in green) and so should have been assigned reduced FSC. This suggests that the agreement between the parametrized and retrieved SO_x emissions will increase with more sophisticated emissions parametrizations. These results demonstrate the possibility of satellite retrievals of ship SO_x emissions under appropriate meteorological conditions.

4. Discussion and Conclusions

The difficulty of isolating the aerosol influence on cloud properties has limited how accurately aerosol-cloud interactions can be constrained by observations. As they are a clear case where the aerosol impact on clouds can be identified, many previous studies have used shiptracks as an experiment of opportunity into aerosol cloud interactions, but have been limited by a lack of information on the driving aerosol perturbation

(Segrin et al., 2007; Christensen & Stephens, 2011; Christensen et al., 2014; Toll et al., 2017; Gryspeerdt et al., 2019). This study links parametrized ship emissions to the resulting shiptracks at a large scale to investigate the factors that control the occurrence and properties of shiptracks.

Using the implementation of FSC controls as an experiment of opportunity, a large reduction in shiptracks is shown between 2014 and 2015 in a region affected by these controls, continuing in 2016 (Figure 1). This suggests that sulfate is a key component for the formation of shiptracks, despite the dominance of organics in ship effluent, although further studies of ship emissions in ECA regions is required to rule out other possibilities, such as changes in the aerosol size distribution. While the presence of liquid cloud is a necessary requirement for the formation of a shiptrack, the background cloud state (particularly N_d) plays almost as important a role as the magnitude of the ship emissions in determining whether a shiptrack forms (Figure 2). Combining the known distributions of N_d and ship SO_x emissions, this suggests that half of shiptracks may be undetected, resulting in an underestimate of the climate impact of shipping (Figure 4). Large uncertainties remain on the size of the underestimate, requiring further investigation into the properties of these currently undetected shiptracks.

The importance of the background state (characterized by N_{cln}) for shiptrack properties means that the N_d perturbation is only weakly correlated to size of the aerosol perturbation (equation (1)). However, this work demonstrates that when the background state is accounted for, there is a close relationship between the N_d enhancement and the ship SO_x emissions (Figure 3a). This allows the ship SO_x emissions to be retrieved when the background state is sufficiently clean (Figure 3b).

By connecting a new data set of ship emissions with satellite observations of cloud properties, this work has clearly demonstrated the central role of sulfate in forming shiptracks and highlighted the potentially significant contribution of undetected shiptracks to the climate impact of shipping. The relationship between shiptrack properties and ship SO_x emissions derived in this work also shows the possibility of the satellite retrieval of ship sulfate emissions by observing the impact of shipping on cloud properties.

Acknowledgments
The authors would like to thank Michael Richardson for assistance in constructing the shiptrack identification application, Peter Lelliott (UCL Energy Institute) for his assistance in preparing the ship emission data, and two reviewers for their helpful comments and suggestions on the manuscript. E. G. was supported by an Imperial College Junior Research Fellowship and a Royal Society University Research Fellowship (URF/R1/191602). F. G. was supported by funding from the Ogden Trust. The MODIS and MERRA-2 data were downloaded from the NASA Goddard Earth Sciences (GES) Data and Information Services Center (DISC). The ERA5 data are from the Copernicus Climate Change Service (C3S) Climate Data Store (CDS). The AIS data were obtained from ExactEarth. The shiptrack identification algorithm is available online (at https://github.com/mattchri/shiptrack_detection_algorithm).

References

AAPA (2015). NAFTA container port rankings 2015 (revised). http://aapa.files.cms-plus.com/Statistics/NAFTA CONTAINER PORT RANKING 2015 revised.pdf, last accessed 12th October 2019.

Abdul-Razzak, H., Ghan, S. J., & Rivera-Carpio, C. (1998). A parameterization of aerosol activation: 1. Single aerosol type. *Journal of Geophysical Research*, *103*(D6), 6123–6131. https://doi.org/10.1029/97JD03735

Albrecht, B. A. (1989). Aerosols, cloud microphysics, and fractional cloudiness. *Science*, *245*(4923), 1227–1230. https://doi.org/10.1126/science.245.4923.1227

Boucher, O., Randall, D. A., Artaxo, P., Bretherton, C., Feingold, G., Forster, P. M., & Zhang, X. Y. (2013). *Clouds and aerosols*: Cambridge University Press. https://doi.org/10.1017/CBO9781107415324.016

Campmany, E., Grainger, R. G., Dean, S. M., & Sayer, A. M. (2009). Automatic detection of ship tracks in ATSR-2 satellite imagery. *Atmospheric Chemistry and Physics*, *19*(6), 1899–1905. https://doi.org/10.5194/acp-9-1899-2009

Christensen, M. W., & Stephens, G. L. (2011). Microphysical and macrophysical responses of marine stratocumulus polluted by underlying ships: Evidence of cloud deepening. *Journal of Geophysical Research*, *116*, D03201. https://doi.org/10.1029/2010JD014638

Christensen, M. W., Suzuki, K., Zambri, B., & Stephens, G. L. (2014). Ship track observations of a reduced shortwave aerosol indirect effect in mixed-phase clouds. *Geophysical Research Letters*, *41*, 6970–6977. https://doi.org/10.1002/2014GL061320

Coakley, J. A., Durkee, P. A., Nielsen, K., Taylor, J. P., Platnick, S., Albrecht, B. A., & Hobbs, P. V. (2000). The appearance and disappearance of ship tracks on large spatial scales. *Journal of the Atmospheric Sciences*, *57*(16), 2765–2778. https://doi.org/10.1175/1520-0469(2000)057<2765:TAADOS>2.0.CO;2

Conover, J. H. (1966). Anomalous cloud lines. *Journal of the Atmospheric Sciences*, *23*(6), 778–785. https://doi.org/10.1175/1520-0469(1966)023<0778:ACL>2.0.CO;2

Durkee, P. A., Chartier, R. E., Brown, A., Trehubenko, E. J., Rogerson, S. D., Skupniewicz, C., & King, M. D. (2000). Composite ship track characteristics. *Journal of the Atmospheric Sciences*, *57*(16), 2542–2553. https://doi.org/10.1175/1520-0469(2000)057<2542:CSTC>2.0.CO;2

Durkee, P. A., Noone, K. J., & Bluth, R. T. (2000). The Monterey Area Ship Track Experiment. *Journal of the Atmospheric Sciences*, *57*(16), 2523–2541. https://doi.org/10.1175/1520-0469(2000)057<2523:TMASTE>2.0.CO;2

Durkee, P. A., Noone, K. J., Ferek, R. J., Johnson, D. W., Taylor, J. P., Garrett, T. J., & Rand, H. (2000). The impact of ship-produced aerosols on the microstructure and albedo of warm marine stratocumulus clouds: A test of MAST hypotheses 1i and 1ii. *Journal of the Atmospheric Sciences*, *57*, 2554–2569. https://doi.org/10.1175/1520-0469(2000)057<2554:TIOSPA>2.0.CO;2

Eriksen, T., Hoye, G., Narheim, B., & Meland, B. J. (2006). Maritime traffic monitoring using a space-based AIS receiver. *Acta Astronautica*, *58*(10), 537–549. https://doi.org/10.1016/j.actaastro.2005.12.016

Goren, T., & Rosenfeld, D. (2012). Satellite observations of ship emission induced transitions from broken to closed cell marine stratocumulus over large areas. *Journal of Geophysical Research*, *117*, D17206. https://doi.org/10.1029/2012JD017981

Grandey, B. S., Stier, P., & Wagner, T. M. (2013). Investigating relationships between aerosol optical depth and cloud fraction using satellite, aerosol reanalysis and general circulation model data. *Atmospheric Chemistry and Physics*, *13*(6), 3177–3184. https://doi.org/10.5194/acp-13-3177-2013

Grosvenor, D. P., Sourdeval, O., Zuidema, P., Ackerman, A., Alexandrov, M. D., Bennartz, R., et al. (2018). Remote sensing of droplet number concentration in warm clouds: A review of the current state of knowledge and perspectives. *Reviews of Geophysics*, *56*, 409–453. https://doi.org/10.1029/2017RG000593

Gryspeerdt, E., Goren, T., Sourdeval, O., Quaas, J., Mülmenstädt, J., Dipu, S., Unglaub, C., Gettelman, A., Christensen, M. (2019). Constraining the aerosol influence on cloud liquid water path. *Atmospheric Chemistry and Physics*, *19*, 5331–5347. https://doi.org/10.5194/acp-19-5331-2019

Gryspeerdt, E., Quaas, J., & Bellouin, N. (2016). Constraining the aerosol influence on cloud fraction. *Journal of Geophysical Research: Atmospheres*, *121*, 3566–3583. https://doi.org/10.1002/2015JD023744

Hobbs, P. V., Garrett, T. J., Ferek, R. J., Strader, S. R., Hegg, D. A., Frick, G. M., & Innis, G. (2000). Emissions from ships with respect to their effects on clouds. *Journal of the Atmospheric Sciences*, *57*(16), 2570–2590. https://doi.org/10.1175/1520-0469(2000)057<2570:EFSWRT>2.0.CO;2

IMO (2002). SOLAS, chapter V, regulation 19.2 – Carriage requirements for shipborne navigational systems and equipment.

IMO (2008). MEPC.176(58) AMENDMENTS TO THE ANNEX OF THE PROTOCOL OF 1997 TO AMEND THE INTERNATIONAL CONVENTION FOR THE PREVENTION OF POLLUTION FROM SHIPS, 1973, AS MODIFIED BY THE PROTOCOL OF 1978 RELATING THERETO (Revised MARPOL Annex VI).

Klein, S. A., & Hartmann, D. L. (1993). The seasonal cycle of low stratiform clouds. *J. Climate*, *6*, 1587. https://doi.org/10.1175/1520-0442(1993)006<1587:TSCOLS>2.0.CO;2

McCoy, D. T., Bender, F. A. M., Mohrmann, J. K. C., Hartmann, D. L., Wood, R., & Grosvenor, D. P. (2017). The global aerosol-cloud first indirect effect estimated using MODIS, MERRA, and AeroCom. *Journal of Geophysical Research: Atmospheres*, *122*, 1779–1796. https://doi.org/10.1002/2016JD026141

Noone, K. J., Johnson, D. W., Taylor, J. P., Ferek, R. J., Garrett, T., Hobbs, P. V., et al. (2000). A case study of ship track formation in a polluted marine boundary layer. *Journal of the Atmospheric Sciences*, *57*, 2748. https://doi.org/10.1175/1520-0469(2000)057<2748:ACSOST>2.0.CO;2

Platnick, S., Meyer, K. G., King, M. D., Wind, G., Amarasinghe, N., Marchant, B., & Riedi, J. (2017). The MODIS cloud optical and microphysical products: Collection 6 updates and examples from Terra and Aqua. *IEEE Transactions on Geoscience and Remote*, *55*(1), 502–525. https://doi.org/10.1109/TGRS.2016.2610522

Possner, A., Wang, H., Wood, R., Caldeira, K., & Ackerman, T. P. (2018). The efficacy of aerosol-cloud radiative perturbations from near-surface emissions in deep open-cell stratocumuli. *Atmospheric Chemistry and Physics*, *18*(23), 17475–17488. https://doi.org/10.5194/acp-18-17475-2018

Quaas, J., Boucher, O., & Lohmann, U. (2006). Constraining the total aerosol indirect effect in the LMDZ and ECHAM4 GCMs using MODIS satellite data. *Atmospheric Chemistry and Physics*, *6*(4), 947–955. https://doi.org/10.5194/acp-6-947-2006

Quaas, J., Stevens, B., Stier, P., & Lohmann, U. (2010). Interpreting the cloud cover-aerosol optical depth relationship found in satellite data using a general circulation model. *Atmospheric Chemistry and Physics*, *10*(13), 6129–6135. https://doi.org/10.5194/acp-10-6129-2010

Randles, C. A., da Silva, A. M., Buchard, V., Colarco, P. R., Darmenov, A., Govindaraju, R., & Flynn, C. J. (2017). The MERRA-2 Aerosol Reanalysis, 1980 onward. Part I: System description and data assimilation evaluation. *Journal Climate*, *30*(17), 6823–6850. https://doi.org/10.1175/JCLI-D-16-0609.1

Rosenfeld, D. (2000). Suppression of rain and snow by urban and industrial air pollution. *Science*, *287*(5459), 1793–1796. https://doi.org/10.1126/science.287.5459.1793

Rosenfeld, D., Liu, G., Yu, X., Zhu, Y., Dai, J., Xu, X., & Yue, Z. (2014). High-resolution (375 m) cloud microstructure as seen from the NPP/VIIRS satellite imager. *Atmospheric Chemistry and Physics*, *14*(5), 2479–2496. https://doi.org/10.5194/acp-14-2479-2014

Russell, L. M., Sorooshian, A., Seinfeld, J. H., Albrecht, B. A., Nenes, A., Ahlm, L., & Wonaschütz, A. (2013). Eastern Pacific Emitted Aerosol Cloud Experiment. *Bulletin of the American Meteorological Society*, *94*, 709–729. https://doi.org/10.1175/BAMS-D-12-00015.1

Schreier, M., Joxe, L., Eyring, V., Bovensmann, H., & Burrows, J. P. (2010). Ship track characteristics derived from geostationary satellite observations on the west coast of southern Africa. *Atmospheric Research*, *95*, 32–39. https://doi.org/10.1016/j.atmosres.2009.08.005

Schreier, M., Mannstein, H., Eyring, V., & Bovensmann, H. (2007). Global ship track distribution and radiative forcing from 1 year of AATSR data. *Geophysical Research Letters*, *34*, L17814. https://doi.org/10.1029/2007GL030664

Segrin, M. S., Coakley, J. A., & Tahnk, W. R. (2007). MODIS observations of ship tracks in summertime stratus off the West Coast of the United States. *Journal of the Atmospheric Sciences*, *64*, 4330. https://doi.org/10.1175/2007JAS2308.1

Smith, T. W. P., Jalkanen, J. P., Anderson, B. A., Corbett, J. J., Faber, J., Hanayama, S., O'Keeffe, E., Parker, S., Johansson, L., Aldous, L., Raucci, C., Traut, M., Ettinger, S., Nelissen, D., Lee, D. S., Ng, S., Agrawal, A., Winebrake, J. J., Hoen, M., Chesworth, S., & Pandey, A. (2015). Third IMO GHG Study 2014; International Maritime Organization (IMO) London, UK, April 2015.

Toll, V., Christensen, M., Gassó, S., & Bellouin, N. (2017). Volcano and ship tracks indicate excessive aerosol-induced cloud water increases in a climate model. *Geophysical Research Letters*, *44*, 12,492–12,500. https://doi.org/10.1002/2017GL075280

Twomey, S. (1959). The nuclei of natural cloud formation part II: The supersaturation in natural clouds and the variation of cloud droplet concentration. *Geofisica Pura e Applicata*, *43*(1), 243–249. https://doi.org/10.1007/BF01993560

Twomey, S. (1974). Pollution and the planetary albedo. *Atmospheric Environment*, *12*(8), 1251–1256. https://doi.org/10.1016/0004-6981(74)90004-3

Zheng, Y., Rosenfeld, D., & Li, Z. (2016). Quantifying cloud base updraft speeds of marine stratocumulus from cloud top radiative cooling. *Geophysical Research Letters*, *43*, 11,407–11,413. https://doi.org/10.1002/2016GL071185